2D Hierarchical Microbarcodes with Expanded Storage Capacity for Optical Multiplex and Information Encryption

Xie, Yujie; Tong, Zaizai; Xia, Tianlai; Worch, Joshua c.; Rho, Julia y.; Dove, Andrew p.; O'reilly, Rachel k.

[Link to publication on Research at Birmingham portal](#)

2D Hierarchical Microbarcodes with Expanded Storage Capacity for Optical Multiplex and Information Encryption

Yujie Xie, Zaizai Tong, Tianlai Xia, Joshua C. Worch, Julia Y. Rho, Andrew P. Dove,* and Rachel K. O'Reilly*

The design of nanosegregated fluorescent tags/barcodes by geometrical patterning with precise dimensions and hierarchies could integrate multilevel optical information within one carrier and enhance microsized barcoding techniques for ultrahigh-density optical data storage and encryption. However, precise control of the spatial distribution in micro/nanosized matrices intrinsically limits the accessible barcoding applications in terms of material design and construction. Here, crystallization forces are leveraged to enable a rapid, programmable molecular packing and rapid epitaxial growth of fluorescent units in 2D via crystallization-driven self-assembly. The fluorescence encoding density, scalability, information storage capacity, and decoding techniques of the robust 2D polymeric barcoding platform are explored systematically. These results provide both a theoretical and an experimental foundation for expanding the fluorescence storage capacity, which is a longstanding challenge in state-of-the-art microbarcoding techniques and establish a generalized and adaptable coding platform for high-throughput analysis and optical multiplexing.

1. Introduction

Barcodes, in which fluorescence forms the basis of the coding, enable an extensive array of encoded signals for high-throughput analysis by arranging and recombining fluorescent signal molecules, and as such, are a leading technique for micro- or nanoscale optical multiplex across the fields of biology, medicine, and materials science.[1] An important development for assay platforms-based microbarcodes is the ability to access a sufficient number of distinct signals with well-defined architectures, which have profound implications including labeling intricate biological molecules, ultrahigh-density optical data storage, and enhancing security inks.[2] However, the general and practical application of fluorescent barcode technologies has remained elusive as a consequence of the challenges related to increasing the accuracy and precision of the stored information (avoiding information overlap and cross-disturbances) while maintaining accessibility and stability (more information on the single carrier).[3] Recent advances to address these limitations have focused on introducing additional coding dimensions (fluorescence lifetime,[4] anisotropy,[5] photoactivation[6]) into each signal carrier to expand the distinguishable coding library.

An array of objects can be marked and tracked by using spatial (width) information in addition to optical information (color/intensity) as an encoding mechanism, similar to bulk barcode design.[7] Multilayered architectures enable the spatial localization of the different information on the single carriers, which could lead to enhanced patterning complexity in an effort to expand the information storage library and high-throughput analysis. Compared to 0D spherical structures, the development of higher-dimensional structures such as 1D cylindrical or 2D platelet morphologies and complex heteromorphologies can decipher a hybrid spectral/graphical encoding platform with the spatial distribution of fluorescent molecules and increase patterning complexity.[8] For example, 1D fluorescent-encoding techniques can define geometric length information into the micro- or nanomatrices by introducing segmented patterns, however the fidelity or accuracy of spatial information is limited due to stochastic changes in material morphology from aggregation, bending, and/or twisting.[9]

2D microstructured materials offer further improvement in information storage, such as patterned signal output with a higher degree of geometric complexation and enhanced accuracy and flexibility of signal processing at the nanoscale.[10] The current state-of-the-art in this area has widely utilized lithographic

Y. Xie, Z. Tong, T. Xia, J. C. Worch, J. Y. Rho, A. P. Dove, R. K. O'Reilly
School of Chemistry
University of Birmingham
Edgbaston, Birmingham B15 2TT, UK
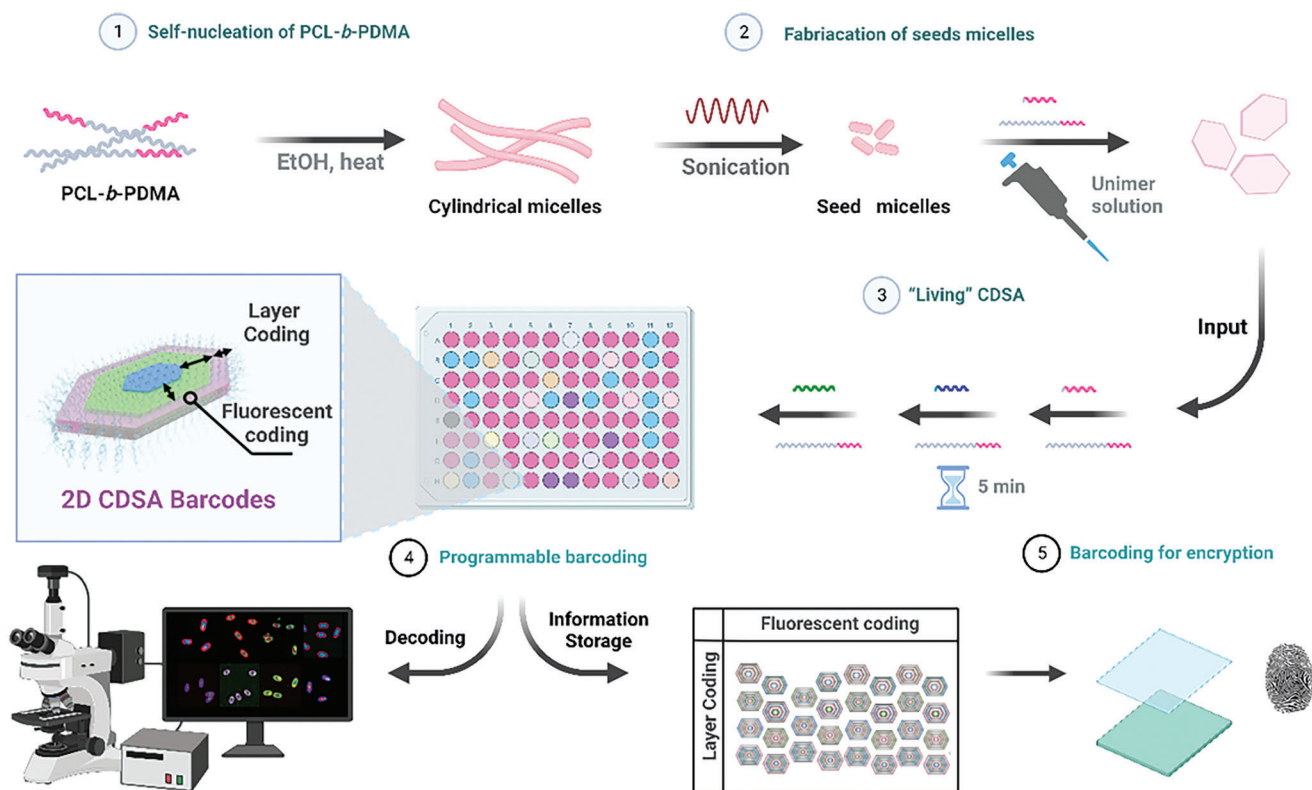E-mail: a.dove@bham.ac.uk; r.oreilly@bham.ac.uk
Y. Xie
School of Medicine
Shanghai University
Shanghai 200444, China
Z. Tong
College of Materials Science and Engineering
Zhejiang Sci-Tech University
Hangzhou 310018, China

**ADVANCED
SCIENCE NEWS**

www.advancedsciencenews.com

**ADVANCED
MATERIALS**

www.advmat.de

Scheme 1. Schematic illustration of design strategy of 2D hierarchical microbarcodes with programmable fluorescent information output via "living" CDSA. Created with http://BioRender.com.

methods to generate precise 2D barcodes. Though these methods can form precise platelets on the microscale, there are clear limitations in resolution that arise, see Table S1 in the Supporting Information.[11] Solution-based systems provide facile methods to access 2D platelet morphologies and are not limited like lithographic resolution. Furthermore, if accuracy could be maintained, these methods would significantly advance the speed and scalability in the synthesis of these complex structures.[12] Efforts to simplify the construction of 2D coding materials while also considering the stability of materials and the accuracy of microstructure control are essential to delivering practical 2D fluorescent coding design.

Conventional polymeric self-assemblies driven by solvophobicity are in highly dynamic equilibrium and intrinsically uncontrolled in one direction, thus assembling strategies to achieve high-dimensional assembly remain rare. Leveraging the living crystallization-driven self-assembly (CDSA) of block copolymers (BCPs) enables the solution assembly of multidimensional nanostructured polymeric materials with a wide structure–property window through the high degree of dimensional, structural, or segmental control.[13] Crystallization as a driving force allows for reducing interfacial curvature, which is particularly favorable for constructing high-dimensional structures such as 1D cylindrical and 2D platelet structures. 1D cylindrical fluorescent microbarcodes with well-defined segments possessing emissive or non-emissive properties have been prepared;[14] however, the addition of a second dimension would significantly increase the pattern com-

plexity and total encoding density to provide a significant step forward in delivering a practical fluorescent barcoding technology. Qui et al. previously introduced a seeded-growth CDSA fabrication method for creating a uniform and monodisperse 2D nanoscale platelet micelles using crystallizable poly(ferrocenyldimethylsilane) polymers. This pioneering work marked the first successful control of the spatial localization of fluorescent units at the nanoscale within polymeric 2D assemblies.[15]

In this study, we report a living seeded growth CDSA method to afford stable hierarchical 2D microbarcodes with ultra-high optical storage capacity and well-defined fluorescent color and patterns due to precise spatial geometric information from programming the addition of each polymer layer (**Scheme 1**). Exquisite control over the layer composition and fluorescence input can be achieved by programming the addition of polymers, leading to a high optical storage capacity. Importantly, this approach allowed for rapid in situ fabrication of nano- to microsized barcodes where more than ten fluorescently encoded layers were formed within 10 min without the need for any postpurification methods. The assemblies displayed robust stability after blending with other polymers, thus demonstrating a proof-of-concept anti-counterfeiting label for plastic materials such as currency. The versatility of this solution-based approach, together with the significant improvements in speed and scale, allow us to significantly advance the practical translation of 2D barcodes for information storage and encryption.

ADVANCED
SCIENCE NEWS

www.advancedsciencenews.com

**ADVANCED
MATERIALS**

www.advmat.de

2. Results and Discussion

2.1. The Design Strategy of 2D Platelets for Barcoding Applications

An efficacious encoding strategy necessitates precision and efficiency, mandating alterations in the *x-y* plane with minimal spatial overlap. The strong directionality of the building blocks plays a crucial role in governing the formation of low-curvature structures during the self-assembly process. In this work, we utilize CDSA as a method to control the directionality and curvature of our platelets. Herein, polycaprolactone (PCL) is selected as core forming block owing to its intrinsic ability to spontaneously crystallize in solution, thereby facilitating the formation of stable, self-assembled nanostructures. The resulting nanostructures comprise of a semi-crystalline PCL and a solvophilic corona block (poly(N,N-dimethylacrylamide), PDMA), which stabilizes the nanostructure in solution.

To optimize the efficiency of the epitaxial growth in CDSA processes, a homopolymer/BCP blending system was applied to prompt epitaxial 2D growth. Within this blend, the homopolymer (which contains PCL only) serves to reduce the overall curvature of the self-assembled nanostructure while the BCP (which contains a crystallizable PCL block and solvophilic PDMA block) stabilizes the resulting nanostructure in solution. Our group recently reported a series of uniform polylactone-based 2D platelets via a diblock copolymer/homopolymer unimer blending strategy.[16] Compared to other polylactone systems, the PCL blending system results in a relatively stable and uniform 2D assembly with well-defined size and morphological control.

To ensure precision and uniformity in the regulation of nanostructures, we implemented a living CDSA process, leveraging short, uniform seeds as prenucleated sites. This strategy promotes uniform and extensive growth of platelets within the solution, maintaining consistency throughout the entirety of the self-assembly process. By employing a programmable addition of multiplex unimers, it crucially facilitate the growth of multilayered platelets with sequence-controlled capability, maintaining the activity at the edges of the assembly. This method, therefore, offers a highly tunable and straightforward construction of multilayered platelets, with the paramount benefit of exceptional platelet regulatability.

2.2. Seeded Growth of 2D Platelets Based on the PCL Blending System

Our experimental setup employed a living CDSA process to fabricate uniform multilayered platelets. The term "living" in this context denotes the capacity of the system to generate uniformly self-assembled structures, with the potential for consistent growth upon the incremental introduction of unimers. To form the first layer, we use a short uniform seed, which provides the prenucleated species from which the self-assembly, driven by crystallization, can occur. Importantly, this strategic approach ensures the immediate commencement of platelet growth following the addition of unimers to the seeded solution. In the case of multilayered platelets, uniform platelets can act as the prenucleated structure, from which further controlled growth can occur. This iterative procedure is key to achieving uniformity across multilay-

ered platelets. The flexibility to manipulate the order of unimer addition in this simplified manner endows us with a remarkably straightforward methodology to tailor the combinations of platelets, subsequently enhancing the order programmability of these nano barcode structures, as illustrated in Figure S11 in the Supporting Information. Additionally, modulating the unimer-to-seed ratio provided an avenue for spatial customization, where an elevated ratio was instrumental in increasing the thickness of the layers.

The 2D microbarcode fabrication process should ideally proceed rapidly (fast assembly speed) and in a simple manner (facile synthetic protocol without purification) while maintaining high fidelity information encoding. To this end, low dispersity PCL homopolymers and PCL-*b*-PDMA block copolymers were synthesized as reported previously[17] (**Figure 1**a and Table S2 and Figures S1–S4, Supporting Information) and fluorescence encoding of the crystallizable polymer (PCL) was accomplished by end-group modification of the PCL (covalent coupling) with borondipyrromethene (BODIPY) dyes that possessed three distinct emission channels, termed BODIPY-R, BODIPY-B, and BODIPY-G (Scheme S1, Supporting Information). Efficient dye conjugation was confirmed by ^{1}H nuclear magnetic resonance (NMR) spectroscopy and size exclusion chromatography (SEC) coupled with ultraviolet (UV) absorbance detection (Figures S1–S4, Supporting Information) and showed that the PCL molecular weight and dispersity ($Đ_M < 1.18$) were well maintained (Figure S1b–d and Table S2, Supporting Information).

This study investigated the seeded growth method in assembling the 2D platelets based on the dye-modified PCL system. The polydispersed cylindrical assemblies were initially fabricated through the self-nucleation of PCL-*b*-PDMA (Figure 1a). The micrometer-long polydispersed cylindrical micelles were formed by heating and cooling the ethanol solution of PCL-*b*-PDMA (5.0 mg mL^{-1}). The solution of polydispersed cylindrical micelles was further sonicated to generate the crystalline seed micelles. The transmission electron microscopy (TEM) analysis, stained by 1% uranyl acetate, revealed the effective generation of polydispersed cylindrical micelles (Figure 1b), and seed micelles with an average length of 68 nm (Figure 1c). Notably, the intermittent sonication resulted in the uniform length of seed micelles, which provided nucleation sites for further seed growth of 2D platelets.

The seeded-growth of the PCL based blending system was initially investigated by sequential addition of a tetrahydrofuran (THF) solution of blended unimer (20 mg mL^{-1}, PCL$_{50}$:PCL$_{50}$-*b*-PDMA$_{200}$ = 1:1, w/w) into a diluted solution (0.01 mg mL^{-1} in ethanol) of crystalline seed micelles. Well-defined 2D platelets were generated within 2 min as confirmed by TEM (Figure 1d) and atomic force microscopy (AFM) micrographs (Figure S5, Supporting Information). The seed growth processes were further confirmed by confocal laser scanning microscope (CLSM) using fluorophorelabeled seed micelles (PCL-*b*-PDMA-G). In lieu of non-fluorescent micelles, the green emission from the seed micelles constructed by PCL-*b*-PDMA-G appeared evenly in the center of platelets, confirming the self-nucleation process that was initiated by adding the blending unimer solution of PCL homopolymer. Meanwhile, the end-group modification of the fluorophores did not affect the 2D morphology (Figure 1f–h). To confirm the localization of the homopolymer and block copolymer on the formed 2D platelets, the combination of dye-modified
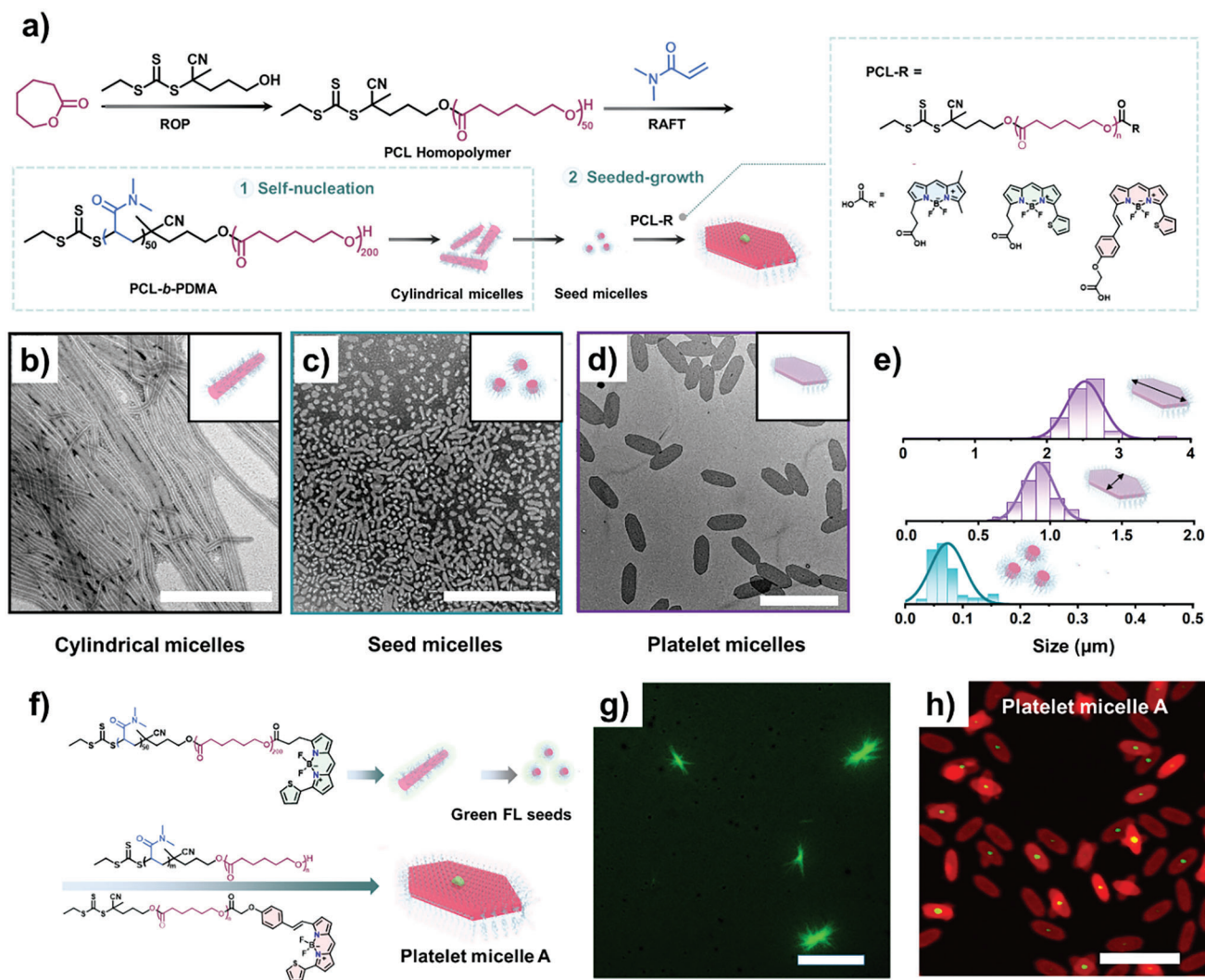
ADVANCED
SCIENCE NEWS
www.advancedsciencenews.com

ADVANCED
MATERIALS
www.advmat.de

Figure 1. a) Illustration of polymer synthesis, seed micelles preparation, and growth process. b–e) TEM micrographs of assemblies illustrating the different morphologies: b) polydispersed cylindrical micelles, c) seed micelles, and d) platelets micelles stained with 1 wt% uranyl acetate in water. e) Size distributions of seed micelles and CDSA platelets calculated from corresponding TEM images, illustrating the morphology and histogram of observed size distributions. f) Schematic representation of the preparation of CDSA platelet micelle A via seed-growth method bearing green boron dipyrromethenes (BODPY) dye-modified seeds and red BODPY dye-modified platelets. g) Confocal micrograph of cylindrical micelles labeled with green emissive dyes. Scale bar: 10 μm. h) Confocal micrograph of formed CDSA platelets labeled with red emissive dyes. Scale bar: 5 μm.

homopolymer and block copolymer (PCL-R and PCL-*b*-PDMA-G) unimer solution was applied during the seeded-growth process, resulting in the merged red channel of PCL-R and the green channel of PCL-*b*-PDMA-G in the resultant platelets without any separation (Figure S5, Supporting Information).

2.3. Kinetics of 2D Epitaxial Growth and Colloidal Stability

The addition of the crystallizable/semi-crystallizable PCL is proposed to self-nucleate in the seed solution or attach to the exposed crystalline end of the seed if undergoing "living" CDSA. Further unimer addition allowed the subsequent sequential living growth of the 2D structures with linear growth being observed upon increasing unimer-to-seed ratios (**Figure 2**a–c). The average length

and width of the resulting 2D micelles were able to be controlled between 0.8 and 2.0 μm while the width varied from 0.4 to 1 μm at unimer-to-seed ratio between 10 and 30 (Table S3, Figure 2f, Figure S6, Supporting Information). The size of the CDSA assembles were confirmed to be proportional to the unimer-to-seed ratio, which indicates the "living" CDSA behavior and epitaxial growth of the PCL blending system. The average area of acquired platelets was analyzed by Image J, which demonstrated the linear increase with the addition of unimer solution (Figure S7, Supporting Information). Notably, the solution of platelets was kept at a narrow length/width dispersity in the presence of PCL blending solution with different unimer-to-seed ratios. No obvious aggregation was observed, establishing a stable and quantifiable system for further barcoding applications. Importantly, no purification steps were conducted over the entirety of the seeded
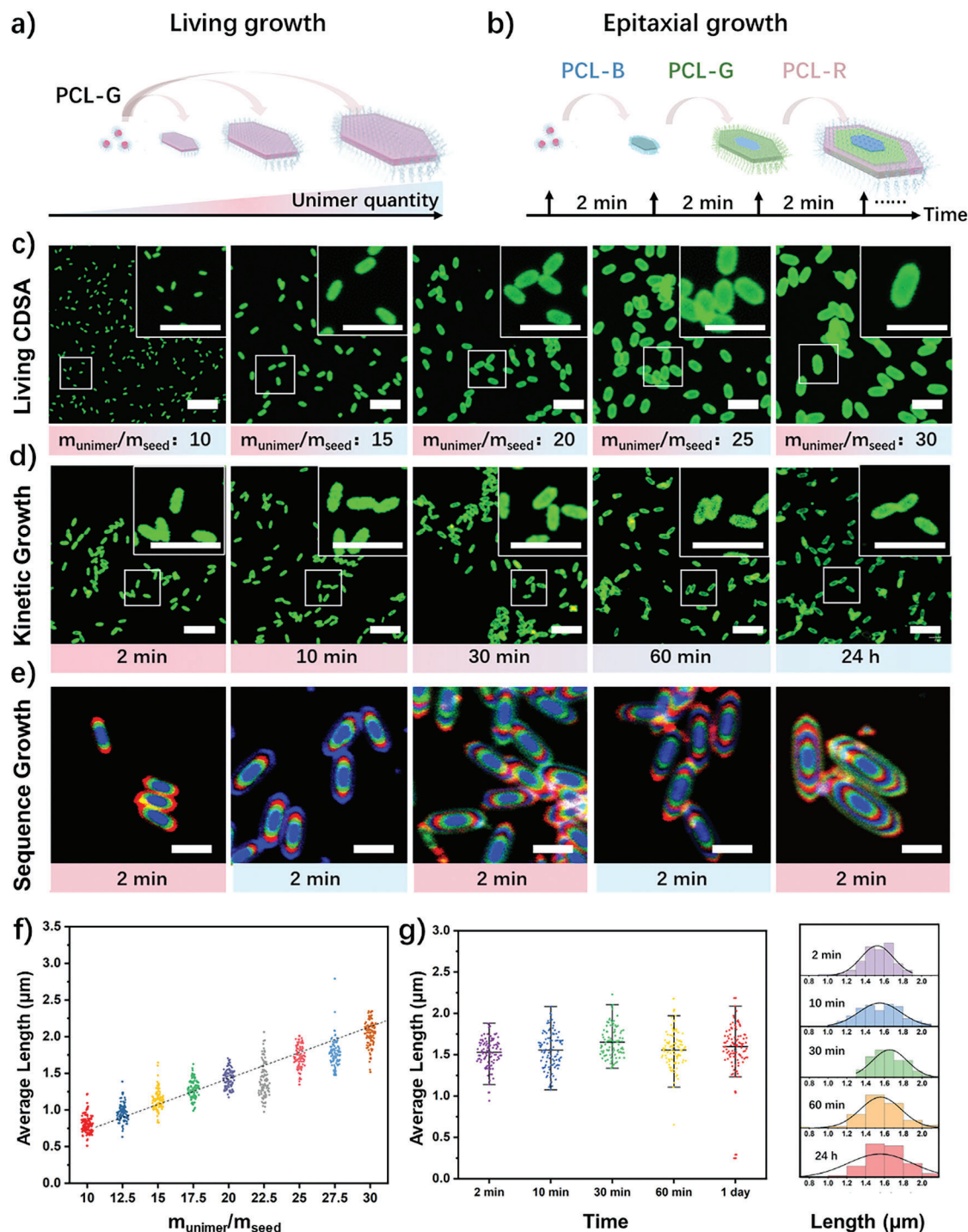
ADVANCED
SCIENCE NEWS

www.advancedsciencenews.com

ADVANCED
MATERIALS

www.advmat.de

Figure 2. a,b) Schematic representation of the mechanism investigation on the living growth and sequential growth of CDSA platelet micelles. c) CLSM images of PCL/PCL-*b*-PDMA (mass ratio = 1) blending platelets grown from PCL-*b*-PDMA crystalline seeds with m_{unimer}/m_{seed} of 10–30 ($C_{seed} = 0.01$ mg mL^{-1}). Scale bar: 4 µm. d) CLSM monitoring of single fragmented platelets from 2 min to 1 d after addition of unimer ($m_{unimer}/m_{seed} = 20$, $C_{seed} = 0.01$ mg mL^{-1}). Scale bar: 4 µm. e) Epitaxial growth of multilayered platelets by sequential addition of different dye-functionalized PCL homopolymers blending solution every 2 min. Scale bar: 1 µm. CLSM illustrated the 2D platelets with segregated regions comprised of different dyes. f) Linear dependence of the length of the single fragmented platelets after the addition of different ratio of unimers (m_{unimer}/m_{seed} of 10–30). g) Plot of the length change of the single fragmented platelets after the formation of 2D platelets from 2 min to 1 d after addition of unimer ($m_{unimer}/m_{seed} = 20$).

2308154 (5 of 13)

**ADVANCED
SCIENCE NEWS**

www.advancedsciencenews.com

**ADVANCED
MATERIALS**

www.advmat.de

growth processes and no obvious background fluorescence was detected from CLSM images, which further supports the high efficiency of the assembly process.

Rapid information writing and effective control over the microstructure are important to realizing practical application of information storage and encryptions.[18] It is, therefore, imperative to evaluate the growth kinetics and size kinetics of the PCL-based CDSA system. The kinetic growth process of the CDSA was tracked microscopically through TEM, where the number/weight average was tracked as a function of time. Uniform 2D micelles were visualized 2 min after adding the PCL-G/PCL-*b*-PDMA blending mixture to the seed solutions.[19] Notably, the same 2D micelles imaged in situ at 10, 30, and 60 min and 24 h resulted in similar 2D structures without obvious change in morphology or uniformity (Figure 2d). The calculated number of average micelle length indicated that the seed growth process of PCL homopolymer/block copolymer was completed within 2 min and there were no further combination/aggregation between formed 2D micelles (Figure 2g).

The effect of concentration on the kinetic growth process was further investigated by decreasing the concentration of seeds and PCL blending. Similarly, the PCL-G/PCL-*b*-PDMA blending solution was added into the CDSA seeds (concentration of 0.005 mg mL^{-1}) under ambient conditions after monitoring the CLSM of the platelets in situ. Interestingly, the platelets were formed after 1 min of injecting PCL blending solution and kept a steady size for 1 min to 2 d (Figure S8, Supporting Information). The growth kinetics of multilayered 2D CDSA system was further investigated by sequentially injecting the different dye-labeled PCL unimer blend solution every 2 min. No obvious overlap between the different layers was observed in the CLSM images of ten cycles of adding dye-labeled PCL blending solutions (Figure 2b,e). In this particular system, the assembly process is incredibly fast, completed in under 2 min. A clear difference in the kinetics of the self-assembly process is observed between the 1D cylindrical and 2D morphologies. Notably, when the unimer solution contains only BCP (PCL-*b*-PDMA), the steric stabilization both leads to higher-curvature morphologies 1D cylinders and slower kinetics. The introduction of homopolymer (PCL), without the sterically bulky corona block, into the unimer solution, leads to less hindered growth, lower curvature 2D platelets and faster assembly kinetics.

To assess the fast kinetic process of 2D growth, we conducted a kinetic study using an aggregation-induced emission (AIEgen) fluorophore (tetraphenylethylene, TPE) modified PCL homopolymer to monitor the assembly process in solution using fluorimetry. The aggregation-induced emission was used to monitor the intramolecular interaction between the PCL chains upon self-assembly. A change in the aggregation state of the AIE dye and emission of the fluorophore was observed between the free unimer and when it was assembled in the 2D platelet.[20] The fluorescence emission spectrum of PCL-TPE/PCL-*b*-PDMA, measured in THF solution at a concentration of 0.02 mg mL^{-1}, exhibited very weak emission at 450–550 nm referring to the free state of the PCL-TPE polymer chain (Figure S9, Supporting Information). In contrast, the addition of PCL-TPE/PCL-*b*-PDMA solution in presence of seed micelles showed a dramatic increase in fluorescence emission, indicating the 2D growth of PCL blending induced the TPE aggregating on the formed platelets. As the con-

trol, the direct addition of PCL-TPE/PCL-*b*-PDMA in the ethanol without the presence of seed micelles led to the polymer precipitation and, as expected, weak emission intensity was observed (Figure S9b, Supporting Information). To monitor the seeded growth process of the TPE-modified PCL system, the steady-state fluorescence was first measured every 5 min for 40 min and then for an additional 20 h with a time interval of 30 min. The intensity of fluorescence emission at 510 nm kept steady, which further confirmed the fast, quantitative formation of platelets and stability of the assembled state. These data further underlined the unique performance of the PCL homopolymer blending system in forming the 2D microscale platelets with extremely fast kinetics, offering an ideal scenario for an effective encoding platform, particularly in expanding the coding patterns and storage capacity.

Aqueous stability was considered by transferring the platelets into water and monitoring in situ under the CLSM (Video S1, Supporting Information). The green fluorescent CDSA platelets were floating in the solution without major aggregation. To confirm the statistical stability of the assembled state, the platelet solution was further monitored by measuring the dynamic light scattering (DLS) at different time intervals. DLS analysis with the correlation function as a function of time confirmed excellent colloidal stability by monitoring from 1 min to 2 weeks (Figure S10, Supporting Information). The unexpected fast kinetics of the polymer growth process is of particular interest in terms of barcoding applications, which could provide economic feasibility in information storage from the perspective of time-cost.

2.4. Evaluation of Barcoding Capacity of 2D CDSA Platelets

The "livingness" property of our PCL blending system in constructing the well-defined 2D platelets with rapid kinetics represents a potential tool in fluorescent barcoding for signal multiplexing and anticounterfeiting. It is envisaged that the patterns on 2D platelets associated with the fluorescence signals as channel designs will be a key strategy in expanding the coding and detection schemes (**Figure 3**a). The color coding was first considered by predesigning the solution of dye-modified PCL before undertaking the CDSA process. PCLs attached to dyes with different primary colors (PCL-Red (R), PCL-Green (G), and PCL-Blue (B)) were mixed in four molar ratios (RGB: 1:1:1, 2:1:1, 1:2:1, 1:1:2) in order to evaluate the capability of color patterning on the single-layer 2D CDSA platelets. The premixed PCL unimer blend solutions with identical concentrations were added to the 0.01 mg mL^{-1} of CDSA seeds solution and the emission color was visualized by CLSM (Figure 3b). The merged channel of the resultant 2D CDSA platelets using CLSM showed four new color patterns. This provides proof-of-concept to illustrate the ability to carefully control the preset color in the single-layered platelets across the whole spectrum, allowing for optimization toward distinct, unique color selections.

Postmixing of the assembled platelets could also allow for multiple information inputs with distinct color codes within one solution, which can be utilized as novel anti-counterfeiting materials with microscopic information. Mixing platelets with three different primary color-codes (Figure 3c, mixed coding 1) and eight different primary color-codes (Figure 3c, mixed coding 2) was
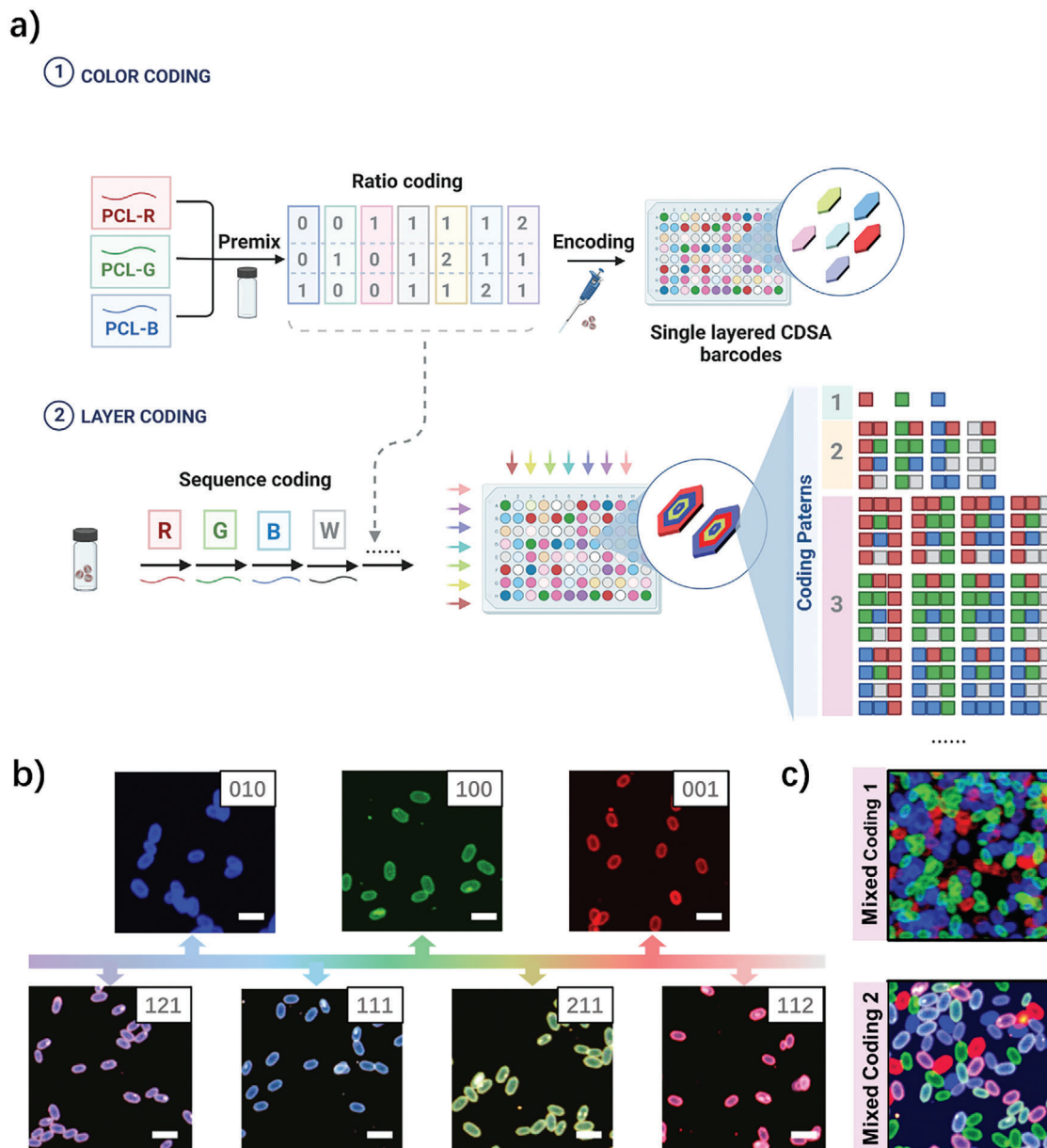
Figure 3. a) Schematic illustration of the two different coding strategies based on the 2D CDSA barcodes. b) CLSM of CDSA barcodes with encoded color information by tuning the distinct ratios of dye labeled PCL unimer solution. Three primary colors (PCL-R, PCL-G, and PCL-B) coded platelets and four ratios premixed primary colors (GBR: 1:1:1, 2:1:1, 1:2:1, 1:1:2) have been visualized in achieving the color patterning on the single-layer 2D CDSA platelets. Scale bar: 4 µm c) The CLSM images of the multiple platelets with three different primary color encoded platelets (mixed coding 1) and eight precoded platelets (mixed coding 2) for a higher level of encryption. The scheme illustration was created with http://BioRender.com.

visualized microscopically and indicated that the color information on each microplatelet was independent of any influence by accumulating different colored platelets together, even at a high concentration of assemblies. The results presented herein highlight an important consideration of 2D structure in fabricating the barcodes rather than 0D spheric and 1D cylindrical structures, in which the 2D pattern provides more stable and reproducible output signals without being affected by aggregating, bending, and twisting of materials at the micro- to nanolevel.[14a,c]

To expand the fluorescence-encoding capacity and achieve a high-security level, the synthesis of 2D micelles with controlled spatial patterns was further investigated using multilayered CDSA platelets (**Figure 4**a). To this end, the incorporation of different color codes (PCL-R, PCL-G, PCL-B) and a white/blank (nonlabeled PCL, as PCL-W) into multiple layers of the 2D micelles with a programmed sequence was targeted. Taking the three-layered CDSA as an example, the encoding capability of different color patterns on the 2D CDSA platelets was first demonstrated by subsequent epitaxial growth of the corresponding
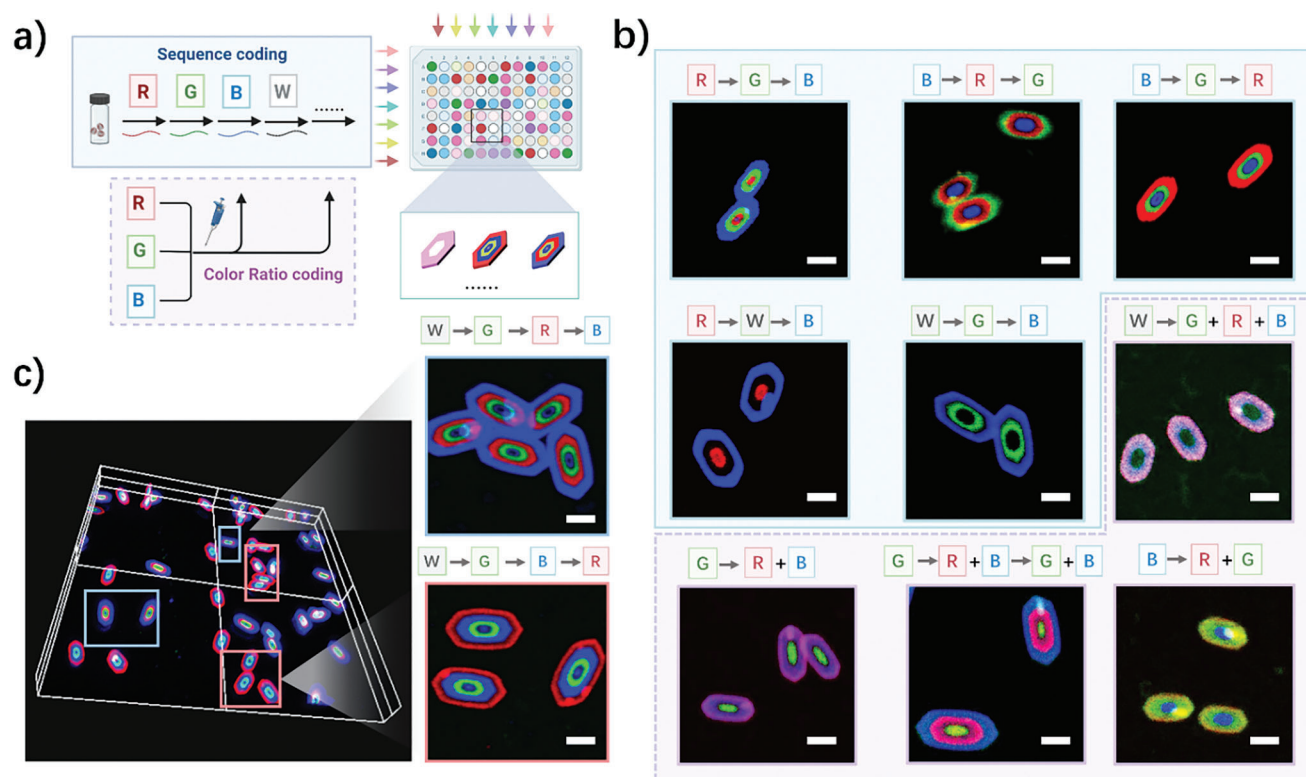
ADVANCED
SCIENCE NEWS
www.advancedsciencenews.com

**ADVANCED
MATERIALS**
www.advmat.de

Figure 4. a) Schematic illustration of the in situ generation of the multisegmented barcodes with programmable encoding patterns on each layer. b) CLSM of examples of programmable two-layered and three-layered CDSA barcodes with spatial localized fluorescent information. G/R/B referred to the different dyes labeled PCL applied and W referred to the PCL without dyes applied. Scale bar: 5 µm. Blue region: Layer coding strategy using the primary color codes. Pink region: Layer coding strategy combined with color coding strategy using the premixed color codes. c) Mixing of two distinct four layers of barcodes (BGRB, BGBR) and visualized under the CLSM without being affected by the aggregation or overlapping. Scale bar: 5 µm. The schematic illustration was created with http://BioRender.com.

PCL blending solution among the presence of CDSA seeds. The green/red/blue/white (G/R/B/W) color was coded on each layer of 2D CDSA in several sequences—B/G/R and R/B/G as examples (Figure 4b)—before the encoded color information was decoded by CLSM, which clearly displayed the color patterns in each layer. This strategy could provide 64 (4*4*4) color patterns for a three layer CDSA platelet when only considering the primary color and layer. Besides using the primary colors, the combination of multiple color within different layers further expands the possibility of coding patterns. For example, the mixed color patterns were encoded in three-layered CDSA platelets with the two patterns as demonstrations: G(R+B), W(G+R+B), G(R+B)(G+B) (Figure 4b).

By varying the sequential addition of unimer, the encoding patterns were further expanded to four-layered CDSA platelets in which the color-coded information can be identified. In this case, the seven different color patterns achieved in the previous section could result in 343 (7*7*7) distinct color codes for three-layer CDSA platelets and 2401 (7*7*7*7) for four-layer CDSA platelets when only considering the primary color and layer. To further evaluate the accuracy and precision of the achieved barcodes, two patterned barcodes with different four layer color designs (B-G-R-B, B-G-B-R) were formed before being mixed within one solution and visualized via CLSM (**Figure 5**c). Owing to the unique 2D patterns, the different layer information coded on the

platelets was distinctly identified without affecting the aggregation or overlapping between the barcodes. The detailed channel information (listed in Figure S11, Supporting Information) and the combination strategies of the color codings and layer codings are further summarized in Figure S12 in the Supporting Information.

2.5. Evaluation of Barcoding Capacity of 2D CDSA Platelets

The decoding capability of the achieved 2D CDSA barcodes was further evaluated microscopically and spectroscopically (Figure 5a), using 13-layered CDSA platelets as a demonstration. The growth of the platelets was achieved by continuously adding different PCL blending solutions and the 13-layered CDSA platelets were achieved within 30 min. The information from each channel (R, B, G) was collected by CLSM analysis (Figure 5b). The decoded information in the different channels provides both well-defined color information and distance information, which potentially provides another variable to further enhance the uniqueness of the pattern. Importantly, macrolevel detecting methods such as fluorescence spectroscopy are insufficient to decode the information contained within the platelets. In order to demonstrate this, four platelet solutions with identical dye quantity but different spatial localization on

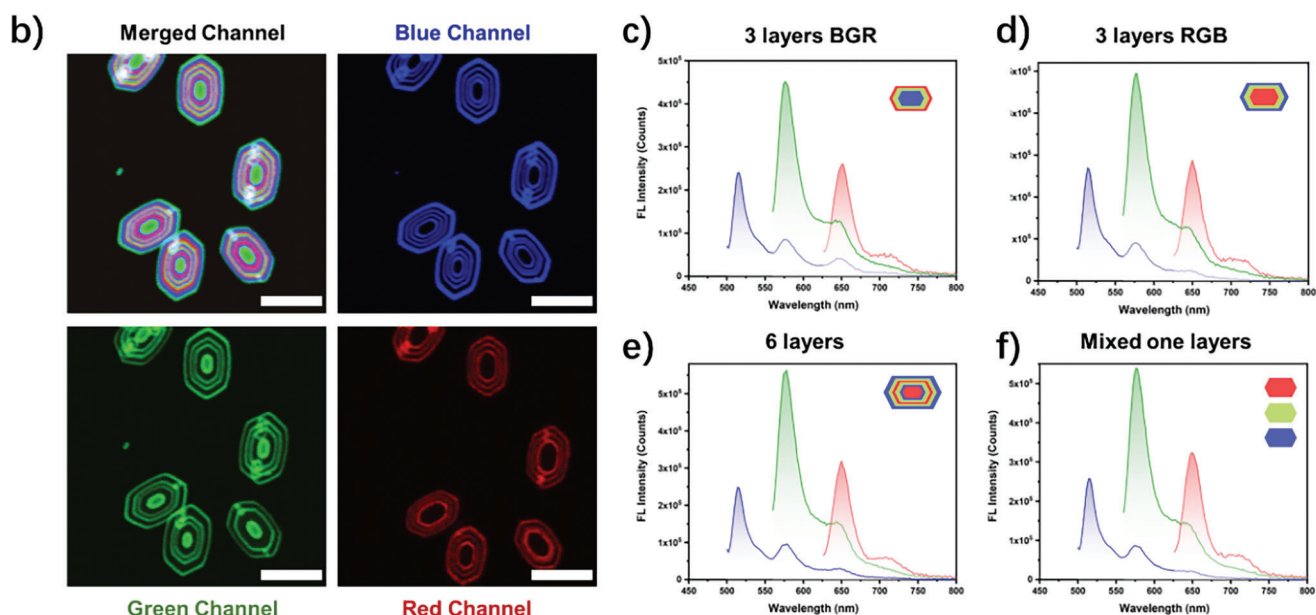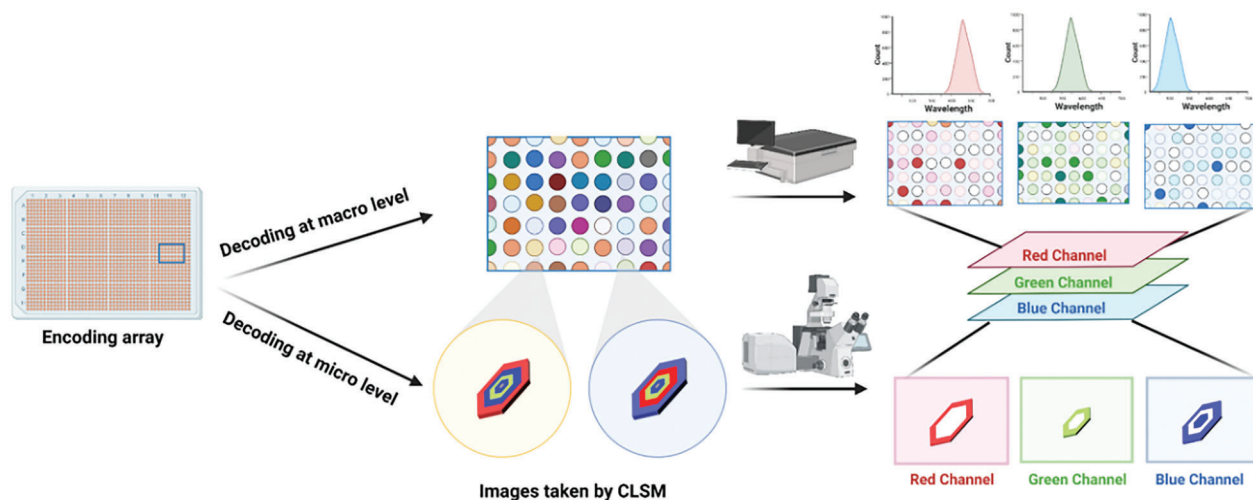## a) DETERMINATION OF THE ENCODED INFORMATION

Figure 5. a) Comparing the decoding techniques applied in this study to identify the information of CDSA barcodes. b) CDSA barcodes which are encoded by 13 layers of fluorescent unimer were decoded by CLSM with different channels of information. Blue channel: λ_{ex}: 488 nm. Green channel: λ_{ex}: 514 nm. Red channel: 630 nm. b–e) Fluorescent spectra of the barcoding systems with the same dye ratios but different coding patterns, including the three-layered c) BGR and d) RGB, e) six-layer RGBRGB and f) mixed single layers. The schematic illustration was created with http://BioRender.com.

the 2D platelets were fabricated. These included changing dye sequences (RGB vs BGR, Figure 5c,d), number of layers (three layers vs six layers, Figure 5e), and simple mixing of single color (nonpatterned) platelets (Figure 5f). The fluorescence spectra of the four platelet solutions were recorded separately after excitation in ethanol solution using the maximum excitation of each dye (Figure S13, Supporting Information). The resulting emission spectra were comparable in each case, as expected, thus proving that the information carried by the single platelets can be identified at the microlevel while the macroscopic characterization cannot reveal the encrypted/encoded information.

2.6. 2D CDSA Platelets as an Anti-counterfeiting Label

The simple and efficient fabrication strategy of such CDSA barcodes with a high variability of the dye composition allows for industrial functions such as anti-counterfeiting. As a proof of concept, 2D particles with predefined fluorescent information were further encapsulated in a polyvinylpyrrolidone (PVP) film to construct an anti-counterfeiting label. Due to the good compatibility between the polymer film and 2D CDSA barcodes, PVP was dissolved into an ethanol solution containing CDSA barcodes and then drop-cast on a glass slide to form the anti-counterfeiting label with encrypted CDSA barcodes. The formed film was
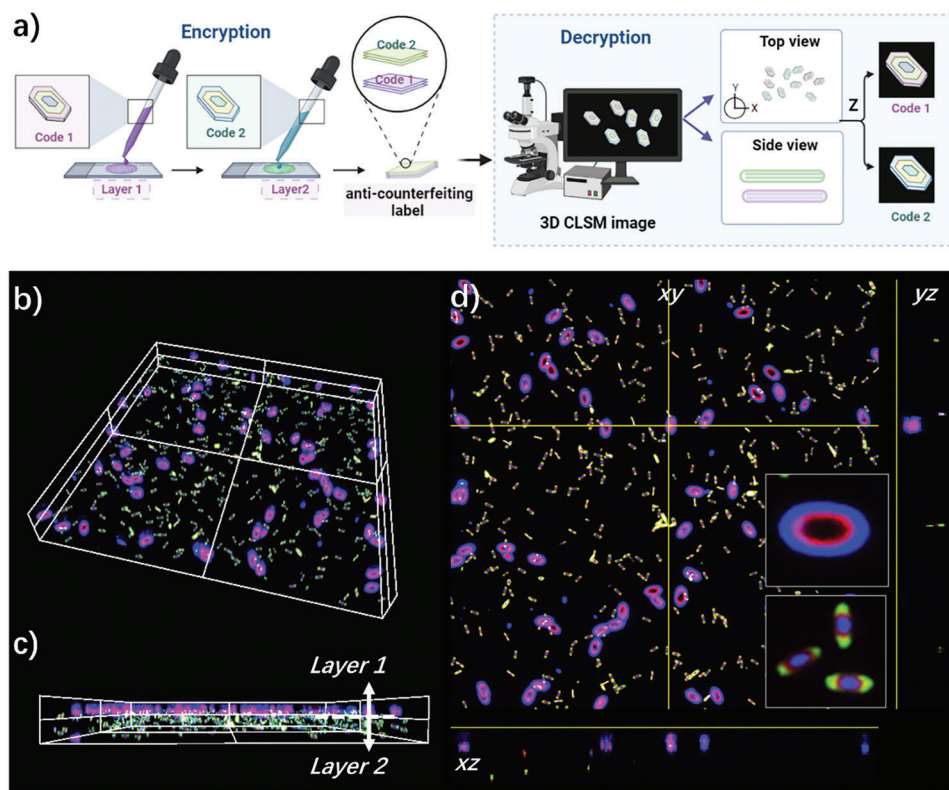
Figure 6. a) Design strategy of the two-layered CDSA anticounterfeiting film bearing different encoded barcodes as anticounterfeiting label. b) 3D reconstruction of *z* scanning CLSM of the encryption PVP film. c) Side view of two-layered CDSA anticounterfeiting film with spatial localized distributions. d) Merged 3D image of *z* scanning CLSM of the encryption PVP film with the enlarged image in the direction of *yz* and *xz*. The schematic illustration was created with http://BioRender.com.

visualized by a layered scanning mode under the CLSM to reconstruct a 3D environment (Figure S14 and Video S2, Supporting Information). Interestingly, the microscaled CDSA barcodes with distinct layer information were distributed evenly in the film and could be identified without any overlap (**Figure 6**). The strong crystallization force led to stable platelets and no disassembly or fluorophore leaking was observed. A two-layered PVP film in which each layer contains 2D barcodes bearing different fluorescent information was targeted to increase the security level of the encryption. This proof-of-concept was achieved by sequential solvent casting and layer scanning CLSM-enabled visualization of the two encrypted CDSA barcodes (Figure 6b,c) in spatially defined locations in the film (Figure 6d–f).

Finally, a solution of 2D CDSA barcodes was further applied with an anti-counterfeiting ink. The ink was formulated by the mixture of 2D CDSA barcodes and PVP in ethanol and applied to a transparent substrate (polymer file or glass slide) as a fingerprint. The use of CLSM allowed for the observation and decoding of the encoded information across various length scales (**Figure 7**) in which the macroscopic pattern, microscopic and nanoscopic information can be sequentially observed. These results further confirmed the 2D CDSA barcodes as anti-counterfeiting films or inks within which the encrypted information can only be decoded with advanced methods. It also suggests that the CDSA barcodes with high synthesis throughput and stable code reproducibility provide a flexible platform for a higher degree of encryption.

3. Conclusion

Herein, we described a simple, yet powerful strategy to fabricate sophisticated 2D microbarcodes that contain geometric localized information. The seeded growth CDSA approach exploits strong crystallization forces to allow rapid, programmable in situ epitaxial growth of fluorescently labeled polymers, allowing for exquisite spatial control over the microsized platelet architectures without the need for washing or purification. Beyond providing a strong driving force for assembly, the crystalline nature of the particles also afforded high kinetic stability to the resultant assemblies, enabling their proof-of-concept demonstration as complex encryption keys for anti-counterfeiting. High-fidelity patterned information was incorporated (layer-by-layer) to enrich simple fluorescence encoding and increase the storage capacity of the fluorescence information at the single-particle level, i.e., distinguishable fluorescent signals from micro to nanoscale in 2D. The nanosegregated fluorescent tags/barcodes possess geometrical patterning with well-defined dimensions and hierarchies that can incorporate multilevel optical information within one carrier to almost infinite levels, providing wide-ranging capabilities to create uniquely coded materials. Such an approach offers a myriad of usage applications for anti-counterfeiting and beyond. The innate biocompatibility of the polymeric system makes it potentially translatable to biological and medical applications where tracking multiple parallel/sequential interactions and
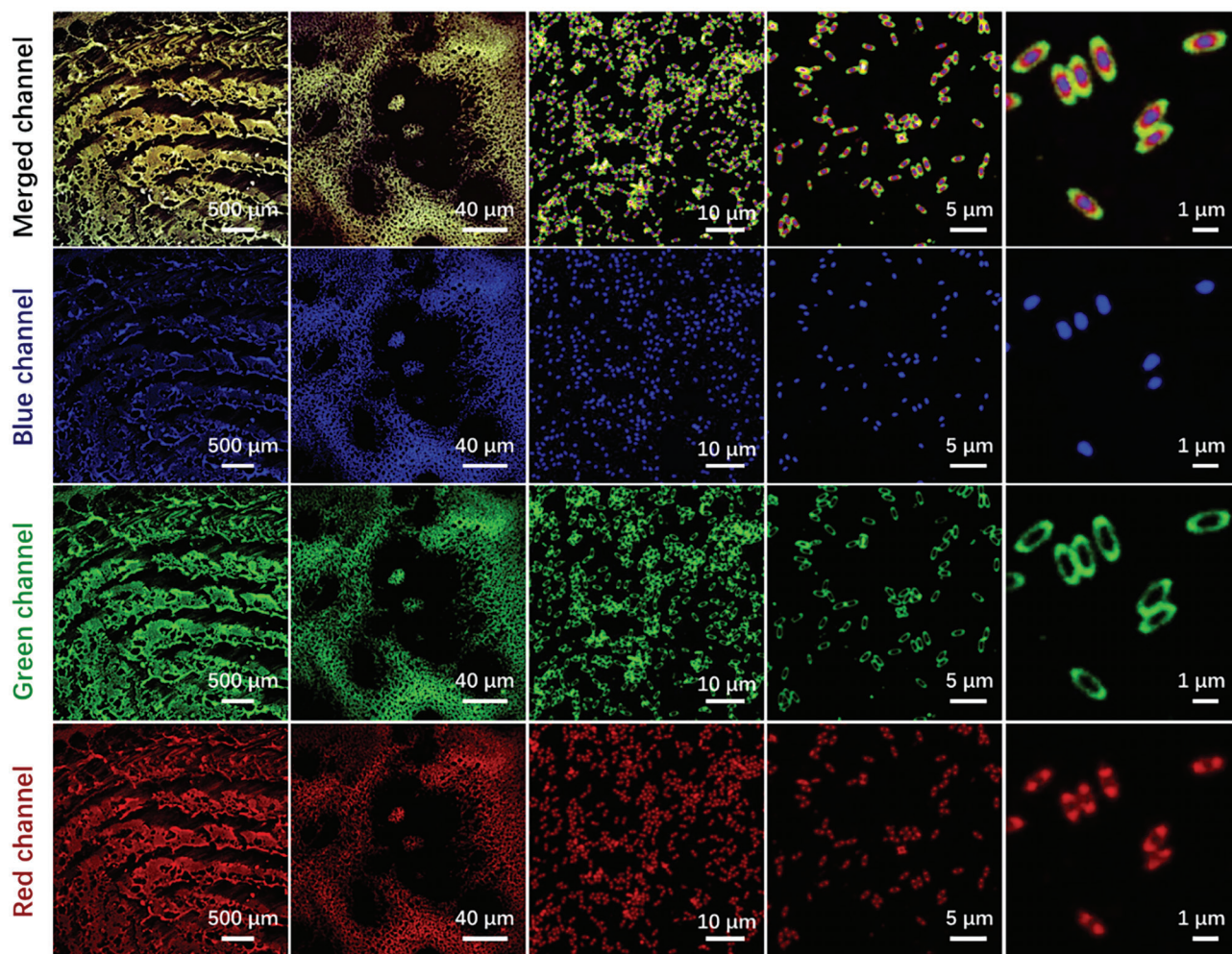
Figure 7. Macroscopic pattern, microscopic and nanoscopic information of the fingerprint encoded by the CDSA anti-counterfeiting ink under the different magnification, collected by CLSM with merge channel, blue channel, green channel, and red channel. Blue channel: λ_{ex}: 488 nm. Green channel: λ_{ex}: 514 nm. Red channel: 630 nm.

expressions of millions of biomolecules is critical to understanding disease or delivering therapeutics.

4. Experimental Section

Materials: Dual-head initiator 2-cyano-5-hydroxypentan-2-yl ethyl carbonotrithioate (chain transfer agent, CTA) was synthesized according to previous reports.[21] Diphenylphosphate (DPP, 99%, Sigma-Aldrich) was recrystallized from dried $CHCl_3$/hexane (3:1). Both CTA and DPP were dried over P_2O_5 in a desiccator under vacuum for 1 week before being introduced in the glovebox and used. ε-caprolactone (99%, ACROS Organics) was vacuum distilled twice over CaH_2 before being introduced in the glovebox and used. 2,2′-Azobis(2-methylpropionitrile) (AIBN, 98%, Sigma-Aldrich) was recrystallized twice from methanol and stored at 4 °C in the dark. *N,N*-dimethyl acrylamide (DMA, 99%, contains 500 ppm monomethyl ether hydroquinone as inhibitor) were purchased from Sigma-Aldrich and passed through a basic alumina plug immediately to remove stabilizer before use. Carboxylic acid derivatives of BODIPY were purchased from Lumiprobe and used directly without further purification. All other chemicals and reagents were purchased from either Sigma-Aldrich, Fisher Chemicals, Acros Chemicals or Alfa Aesar and used

as received. 1,4-Dioxane (anhydrous, 99.8%) was purchased from Fisher Scientific and was purified via passage through a column of basic alumina prior to use. Toluene, Dichloromethane (DCM), and other dry solvents were used directly from the drying and degassing inert solvent system.

Instrumentation: *NMR Spectroscopy*: ^{1}H-NMR and ^{13}C-NMR spectra were recorded on a Bruker DPX-300 and a Bruker DPX-400 spectrometer at 300 and 400 MHz at 298 K, using chloroform-*d* ($CDCl_3$) as the solvent. Chemical shifts are quoted as δ in parts per million (ppm) and are relative to internal standard tetramethylsilane at δ = 0 ppm.

SEC: SEC analysis was performed on an Agilent 1260 Infinity II LC system fitted with refractive index and UV detectors, equipped with an Agilent guard column (PLGel 5 μm, 50 × 7.5 mm²) and two Agilent Mixed-C columns (PLGel 5 μm, 300 × 7.5 mm²). The mobile phase used was high-performance liquid chromatography (HPLC)-grade chloroform containing 0.5% v/v triethylamine at 40 °C at a flow rate of 1.0 mL min⁻¹. The UV detector was set to 309 nm for unfunctionalized polymer whereas the wavelength was changed to 530, 550, and 630 nm, respectively. SEC data were calibrated against poly(methyl methacrylate) (PMMA) standards. The number-average molecular weights (M_n), weight-average molecular weights (M_w), and dispersity ($Đ_M = M_w/M_n$) were determined using the Agilent SEC software.

**ADVANCED
SCIENCE NEWS**

www.advancedsciencenews.com

**ADVANCED
MATERIALS**

www.advmat.de

DLS: DLS was used to detect multiple populations and obtain dispersity information using a Malvern Zetasizer Nano ZS with a 4 mW He-Ne 633 nm laser module operating at 25 °C. Measurements were carried out at an angle of 173° and results were analyzed using Malvern DTS v7.03 software. All determinations were repeated four times with 15 measurements recorded for each run.

TEM: Dry-state stained TEM imaging was performed on a JEOL 1400 transmission electron microscope operating at 80 kV. Samples for TEM analysis were prepared by drop casting 5 μL of the sample (0.005 mg mL^{-1}) onto formvar-coated copper grids. For small-sized samples (seeds per cylinders), the grides were further stained with an aqueous solution of 1 wt% uranyl acetate for 1 min for better microscopic analysis. The average size of the micelles was calculated and analyzed for more than 100 particles using the software ImageJ in each case.

AFM: AFM was performed on a JPK Nanowizard 4 system in alternate contact (tapping) mode. The tips for the AFM analysis (PPP-NCHAuD) were purchased from NANOSENSORSTM, with resonance frequency (kHz) in the window of 204–497 and force constant in the range of 10–130. Samples were prepared by drop-casting 10 μL of the micellar solution onto the silicon wafer. The average size and height information from AFM pictures were analyzed and collected using the JPK Data Processing software with QI mode.

Steady-State Fluorescence Spectroscopy: All steady-state spectra were obtained from Edinburgh Instruments FS5 spectrofluorometer equipped with a Xenon lamp. The solutions of the samples were measured in 10 mm path-length quartz cuvettes with four transparent polished faces (Starna Cells, type: 3-Q-10). The acquired steady-state fluorescence excitation and emission spectra were analyzed in Origin 2019 (Origin Labs).

Confocal Laser Scanning Microscopy (CLSM): CLSM was performed on an FV3000 (Olympus) confocal laser scanning microscope system with an IX-81 inverted base (Olympus) and the 20x and 60x oil lens (Olympus), equipped with 405, 488, 514, and 640 nm laser. The FV3000 system was driven with the FV31S-SW Viewer software platform (Olympus) with scan rates of 1 μs per pixel at 1024 by 1024 pixels. Dry state CLSM images were acquired by deposition of sample solution (0.005 mg mL^{-1}) on a glass slide and imaged by CLSM after evaporation of the solvent. Solution state CLSM images and film samples were measured directly on the glass slides and 3D images were visualized by automatic step scan by changing the *Z* position. Samples were imaged at 60× magnification upon excitation using a $\lambda_{ex} = 488$ nm laser (blue channel, $\lambda_{em} = 505$–530 nm) 514 nm (green channel, $\lambda_{em} = 560$–600 nm), and 640 nm laser (red channel, $\lambda_{em} = 645$–700 nm). 2D and 3D images were processed using cellSens (Olympus) and ImageJ image processing software.

Material Synthesis: *Synthesis of Poly(ε-caprolactone) Homopolymer as Crystalline Core-Forming Blocks*: The PCL$_{50}$ homopolymer was synthesized through a typical ring opening polymerization of ε-caprolactone operated in inert nitrogen glove box. Generally, the DPP (20 mg, 0.08 mmol) and dual-head initiator 2-cyano-5-hydroxypentan-2-yl ethyl carbonotrithioate (20 mg, 0.08 mmol) were dissolved in dry toluene (2 mL) and transferred into ε-caprolactone (543.3 mg, 4.76 mmol, 70 eq) solution toluene (3 mL). After stirring for 6 h at room temperature, the solution was removed from the glove box, precipitated three times into cold diethyl ether dropwise and collected by centrifugation. Chloroform was added to dissolve solids and the polymer was precipitated in cold diethyl ether three times. ^{1}H NMR (400 MHz, CDCl$_3$): δ 4.12 (t, $J = 6.2$ Hz, 2H, CH_2OCO), 4.06 (t, $J = 6.7$ Hz, 101H, CH$_2$CH_2O), 3.65 (t, $J = 6.5$ Hz, 2H, C(CN)CH_2CH$_2$), 3.35 (q, $J = 7.4$ Hz, 2H, SCH_2CH$_3$), 2.39–2.23 (m, 108H, OCOCH_2CH$_2$), 1.89 (s, 3H, C(CN)(CH_3)CH$_2$), 1.72–1.60 (m, 211H, OCOCH$_2$CH_2CH$_2$CH_2), 1.39 (tt, $J = 10.5$, 6.5 Hz, 109H, OCOCH$_2$CH$_2$CH_2CH$_2$). SEC (CHCl$_3$, PMMA standard): $M_n = 16.0$ kg mol^{-1}, $Đ_m = 1.07$.

Synthesis of Diblock Copolymer by Chain Extension of Crystalline Core-Forming Blocks: The diblock copolymer PCL$_{50}$-*b*-PDMA$_{200}$ was synthesized by Reversible addition-fragmentation chain transfer (RAFT) polymerization. PCL$_{50}$ (900 mg, 0.14 mmol), DMA (2.88 g, 29 mmol), and AIBN (2.4 mg, 0.014 mmol) were dissolved in 1,4-dioxane (6 mL) and added to a dry ampoule containing a stirrer bar. The resulting solution was degassed using at least three freeze–pump–thaw cycles, back-filled with nitrogen, sealed and placed in a preheated oil bath at 70 °C. The solution was heated for 2 h at 70 °C and then quenched by immersion of the ampoule in liquid nitrogen. The polymer was precipitated in ice-cold diethyl ether three times before being dried under vacuum and analyzed.

^{1}H NMR (400 MHz, CDCl$_3$) δ 4.08 (t, $J = 6.7$ Hz, CH_2OH), 3.27–2.38 (m, N(CH_3)$_2$, CHCH$_2$ from PDMA), 2.33 (t, $J = 7.5$ Hz, OCOCH_2CH$_2$ from PCL), 2.03–1.11 (m, 223H OCOCH$_2$, OCO(CH_2)$_5$OH from PCL, CHCH_2 from PDMA). SEC (CHCl$_3$, PMMA standard): $M_n = 42.4$ kg mol^{-1}, $Đ_m = 1.18$.

Fluorescent Modification of Polymers: Three different carboxylic-functionalized BODIPY dyes (BODIPY 630/650, BOPIPY R6G, BODIPY FL) were selected to modify three different core domains of PCL. PCL$_{40}$ (50 mg, 9.3 μmol, 2 eq), BODIPY 630/650 (3.3 mg, 9.3 μmol 1eq), 4-dimethylaminopyridine (0.56 mg, 4.6 μmol 0.1), and dicyclohexylcarbodiimide (17.9 mg, 93 μmol 1.1) were dissolved in 2 mL dichloromethane and stirred for 24 h. The reaction mixture was precipitated in cold MeOH three times to yield the end-functionalized fluorescently labeled polymer.

Synthesis of Seeds Micelle: PCL-*b*-PDMA (5 mg) was dissolved into 1 mL of ethanol (5.0 mg mL^{-1}) in a vial and followed by heating at 70 °C for 3 h. The solution was slowly cooled to room temperature and further aged for 5 d to yield micrometer-long polydisperse cylinders. The acquired crystalline cylinders were sonicated in an ice bath for 20 min (ten cycles of 2 min sonication each cycle with an interval of 20 min to cool down the solution temperature) using a sonication probe to fabricate the seed micelles.

Self-Assembly of CDSA Platelets: Epitaxial growth of the PCL blending on the crystalline seeds: the PCL blending solution was first prepared by rapidly mixing the PCL$_{50}$ homopolymer (or 1% dye labeled PCL) and PCL$_{50}$-*b*-PDMA$_{200}$ with a weight ratio of 1:1 in THF (10 mg mL^{-1} and 20 mg mL^{-1}). The CDSA platelets were synthesized by rapid adding a certain volume of PCL blending solution into crystalline seeds (0.01 mg mL^{-1}) and shaking the solution for 5 s. The unimer-to-seed ratio was altered by adding different amounts of unimer solution to the dispersion of seed micelles.

Film Preparation and Macroscopic Pattern: PVP (5000 Da) was dissolved in ethanol followed by sonication to achieve the clear PVP solution. The preformed CDSA platelets (0.1 mg mL^{-1}) were added to the PVP solution followed by drop casting on a glass slide and left to dry overnight. The formed film was analyzed in situ by layered scan on CLSM. The two-layered film was prepared using the same protocol by drop casting another CDSA platelets solution on the top of the formed film.

Fingerprint images were obtained to showcase the application of 2D micro barcodes as anticounterfeiting inks. A mixture of PVP and selected 2D CDSA barcodes in ethanol solution was prepared and a specific amount of ink was manually applied and pressed onto the surface of a transparent object for fluorescent decoding. The encoded fingerprint was then decoded using CLSM, allowing for observation and decoding of the encoded information at different length scales.

Supporting Information

Supporting Information is available from the Wiley Online Library or from the author.

Acknowledgements

Conflict of Interest

The authors declare no conflict of interest.

Data Availability Statement

The data that support the findings of this study are available from the corresponding author upon reasonable request.

[1] a) X. Qiu, J. Xu, M. Cardoso Dos Santos, N. Hildebrandt, *Acc. Chem. Res.* **2022**, *55*, 551; b) X. Zhang, G. Chen, F. Bian, L. Cai, Y. Zhao, *Adv. Mater.* **2019**, *31*, 1902825; c) K. Huang, N. M. Idris, Y. Zhang, *Small* **2016**, *12*, 836; d) F. Lan, B. Demaree, N. Ahmed, A. R. Abate, *Nat. Biotechnol.* **2017**, *35*, 640; e) G. Lin, M. A. B. Baker, M. Hong, D. Jin, *Chem* **2018**, *4*, 997; f) N. R. Visaveliya, J. M. Köhler, *Adv. Opt. Mater.* **2021**, *9*, 2002219; g) Z. Lin, J. Zhou, Y. Qu, S. Pan, Y. Han, R. P. M. Lafleur, J. Chen, C. Cortez-Jugo, J. J. Richardson, F. Caruso, *Angew. Chem., Int. Ed.* **2021**, *60*, 24968; h) F. Hu, C. Zeng, R. Long, Y. Miao, L. Wei, Q. Xu, W. Min, *Nat. Methods* **2018**, *15*, 194.

[2] a) S. Shikha, T. Salafi, J. Cheng, Y. Zhang, *Chem. Soc. Rev.* **2017**, *46*, 7054; b) D. Jin, P. Xi, B. Wang, L. Zhang, J. Enderlein, A. M. Van Oijen, *Nat. Methods* **2018**, *15*, 415.

[3] a) X. Li, Y. Xie, B. Song, H.-L. Zhang, H. Chen, H. Cai, W. Liu, Y. Tang, *Angew. Chem., Int. Ed.* **2017**, *56*, 2689; b) M. Yang, Y. Liu, X. Jiang, *Chem. Soc. Rev.* **2019**, *48*, 850.

[4] Y. Xie, M. C. Arno, J. T. Husband, M. Torrent-Sucarrat, R. K. O'reilly, *Nat. Commun.* **2020**, *11*, 2460.

[5] a) W. Huang, Y. Cheng, J. Zhai, Y. Qin, W. Zhang, X. Xie, *Analyst* **2023**, *148*, 4406; b) Q. Huang, B. Chen, J. Shen, L. Liu, J. Li, J. Shi, Q. Li, X. Zuo, L. Wang, C. Fan, J. Li, *J. Am. Chem. Soc.* **2021**, *143*, 10735.

[6] C. Guo, J. Zhai, Y. Wang, X. Du, Z. Wang, X. Xie, *Anal. Chem.* **2022**, *94*, 1531.

[7] Y. Yan, Y. S. Zhao, *Chem. Soc. Rev.* **2014**, *43*, 4325.

[8] S. Wen, Y. Liu, F. Wang, G. Lin, J. Zhou, B. Shi, Y. D. Suh, D. Jin, *Nat. Commun.* **2020**, *11*, 6047.

[9] a) Z. Gao, B. Xu, T. Zhang, Z. Liu, W. Zhang, X. Sun, Y. Liu, X. Wang, Z. Wang, Y. Yan, F. Hu, X. Meng, Y. S. Zhao, *Angew. Chem., Int. Ed.* **2020**, *59*, 19060; b) V. Pan, W. Wang, I. Heaven, T. Bai, Y. Cheng, C. Chen, Y. Ke, B. Wei, *ACS Nano* **2021**, *15*, 15892; c) C. Lin, R. Jungmann, A. M. Leifer, C. Li, D. Levner, G. M. Church, W. M. Shih, P. Yin, *Nat. Chem.* **2012**, *4*, 832.

[10] a) H. Lee, J. Kim, H. Kim, J. Kim, S. Kwon, *Nat. Mater.* **2010**, *9*, 745; b) A. Rajak, A. Das, *Angew. Chem., Int. Ed.* **2022**, *61*, e202116572; c) Y. Gong, C. Cheng, H. Ji, Y. Che, L. Zang, J. Zhao, Y. Zhang, *J. Am. Chem. Soc.* **2022**, *144*, 15403.

[11] a) L. Hu, Y. Fan, L. Liu, X. Li, B. Zhao, R. Wang, P. Wang, A. M. El-Toni, F. Zhang, *Adv. Opt. Mater.* **2017**, *5*, 1700680; b) D. C. Pregibon, M. Toner, P. S. Doyle, *Science* **2007**, *315*, 1393.

[12] a) J. I. Deneff, K. S. Butler, L. E. S. Rohwer, C. J. Pearce, N. R. Valdez, M. A. Rodriguez, T. S. Luk, D. F. Sava Gallis, *Angew. Chem., Int. Ed.* **2021**, *60*, 1203; b) Y. Liu, Y. Zhang, *ACS Nano* **2021**, *15*, 7628; c) Z. Gao, S. Yang, B. Xu, T. Zhang, S. Chen, W. Zhang, X. Sun, Z. Wang, X. Wang, X. Meng, Y. S. Zhao, *Angew. Chem., Int. Ed.* **2021**, *60*, 24519.

[13] a) X. Wang, G. Guerin, H. Wang, Y. Wang, I. Manners, M. A. Winnik, *Science* **2007**, *317*, 644; b) A. K. Pearce, T. R. Wilks, M. C. Arno, R. K. O'reilly, *Nat. Rev. Chem.* **2021**, *5*, 21; c) L. Macfarlane, C. Zhao, J. Cai, H. Qiu, I. Manners, *Chem. Sci.* **2021**, *12*, 4661; d) S. Ganda, M. H. Stenzel, *Prog. Polym. Sci.* **2020**, *101*, 101195; e) X. He, M.-S. Hsiao, C. E. Boott, R. L. Harniman, A. Nazemi, X. Li, M. A. Winnik, I. Manners, *Nat. Mater.* **2017**, *16*, 481.

[14] a) F. He, T. Gädt, I. Manners, M. A. Winnik, *J. Am. Chem. Soc.* **2011**, *133*, 9095; b) Z. M. Hudson, C. E. Boott, M. E. Robinson, P. A. Rupar, M. A. Winnik, I. Manners, *Nat. Chem.* **2014**, *6*, 893; c) Z. M. Hudson, D. J. Lunn, M. A. Winnik, I. Manners, *Nat. Commun.* **2014**, *5*, 3372.

[15] H. Qiu, Y. Gao, C. E. Boott, O. E. C. Gould, R. L. Harniman, M. J. Miles, S. E. D. Webb, M. A. Winnik, I. Manners, *Science* **2016**, *352*, 697.

[16] Z. Tong, Y. Xie, M. C. Arno, Y. Zhang, I. Manners, R. K. O'reilly, A. P. Dove, *Nat. Chem.* **2023**, *15*, 824.

[17] Z. Tong, Y. Su, Y. Jiang, Y. Xie, S. Chen, R. K. O'reilly, *Macromolecules* **2021**, *54*, 2844.

[18] a) X. Liu, W. Wu, D. Cui, X. Chen, W. Li, *Adv. Mater.* **2021**, *33*, 2004734; b) J. Zhang, S. Shikha, Q. Mei, J. Liu, Y. Zhang, *Mikrochim. Acta* **2019**, *186*, 361.

[19] C. E. Boott, E. M. Leitao, D. W. Hayward, R. F. Laine, P. Mahou, G. Guerin, M. A. Winnik, R. M. Richardson, C. F. Kaminski, G. R. Whittell, I. Manners, *ACS Nano* **2018**, *12*, 8920.

[20] J. Mei, N. L. C. Leung, R. T. K. Kwok, J. W. Y. Lam, B. Z. Tang, *Chem. Rev.* **2015**, *115*, 11718.

[21] M. C. Arno, M. Inam, Z. Coe, G. Cambridge, L. J. Macdougall, R. Keogh, A. P. Dove, R. K. O'reilly, *J. Am. Chem. Soc.* **2017**, *139*, 16980.